

We are IntechOpen, the world's leading publisher of Open Access books Built by scientists, for scientists

6,900

Open access books available

186,000

International authors and editors

200M

Downloads

Our authors are among the

154

Countries delivered to

TOP 1%

most cited scientists

12.2%

Contributors from top 500 universities



WEB OF SCIENCE™

Selection of our books indexed in the Book Citation Index
in Web of Science™ Core Collection (BKCI)

Interested in publishing with us?
Contact book.department@intechopen.com

Numbers displayed above are based on latest data collected.
For more information visit www.intechopen.com



High Entropy Alloys for Medical Applications

*Victor Geanta, Ionelia Voiculescu, Petrica Vizureanu
and Andrei Victor Sandu*

Abstract

A wide variety of metallic biomaterials have been developed so far, including various types of alloys. However, there is a strong need in the medical field for new solutions in what concerns metallic biomaterials with superior biocompatibility and mechanical properties in order to meet future requirements, including the recently developed high entropy alloys (HEAs). This chapter presents some characteristics of high entropy biocompatible metallic alloys produced in an electric-arc remelting furnace in argon inert atmosphere. The effects of the chemical elements used, the microstructural features, and some mechanical characteristics, both in the cast state or after some heat treatments, are highlighted.

Keywords: high entropy alloys, biocompatible, microstructure, microhardness

1. Introduction

1.1 Background

HEAs are defined as alloys comprising more than five main elements mixed in an equiatomic or near-equiatomic fraction [1–14]. Many HEAs have been reported to have: superior mechanical properties, such as ultrahigh fracture even at high temperatures, high hardness, toughness exceeding that of most pure metals and alloys, excellent comparable strength to that of structural ceramics and some metallic glasses, exceptional ductility, and fracture toughness at cryogenic temperatures [1, 3], and good physical properties, such as superconductivity, supermagnetism, and significant resistance to corrosion [5].

By replacing one or several elements in the composition of high entropy alloys, properties that significantly differ from the initial ones can be obtained. Furthermore, the decrease or increase in the ratio of additional elements can generate different metallographic structures with significant influences on the properties of alloys [6–10]. While high-strength conventional alloys are based mainly on the controlled distribution of one or two high-hardness phases at most, in high entropy alloys, the exceptional properties are based on the quenching effect of the supersaturated solid solution and on the suppression of the intermetallic phases [1, 4–12]. The complex distribution of the various chemical elements within the crystalline network of high entropy alloys appears to be the main cause of their special characteristics when compared to the classical or bi-component alloys. Choosing the combination of chemical elements could allow to simultaneously cumulate superior mechanical properties

as well as to ensure special corrosion resistance and biocompatibility, making their use as a new class of biocompatible metallic materials suitable [10, 12].

According to the most recent evaluations, the criteria for forming simple solid solutions in high entropy alloys must comply with the following conditions [13, 14]:

- Configuration entropy (ΔS_{am}), which in cases of high entropy alloys must be higher than 11 J/mol K. The entropy of mixing [Eq. (1)] is calculated using Boltzmann's formula:

$$\Delta S_{mix} = -R \sum c_i \ln c_i \quad (1)$$

where R is the gas constant (8.314 J/mol K) and c_i is the molar fraction of element i.

- The enthalpy of mixing (ΔH_{am}) of the alloy must be between -11.6 and 3.2 kJ/mol, and it is calculated using the derived formula [Eq. (2)] from Miedema's macroscopic model:

$$\Delta H_{am} = \sum c_i c_j \Delta H_{ij} \quad (2)$$

where ΔH_{ij} is the binary enthalpy of the formation of the elements i and j.

- The atomic radius difference criterion (δ), which claims that the phases that contain predominantly solid solutions are formed for values lower than 6.6%, and at values lower than 4%, only solid solutions are formed. The calculation formula Eq. (3) for δ was defined as follows:

$$\delta = 100 \sqrt{\sum c_i \left(1 - \frac{r_i}{\bar{r}}\right)^2} \quad (3)$$

where r_i is the atomic radius of element i and \bar{r} is the average atomic radius.

- The derived parameter Ω includes ΔS_{am} and ΔH_{am} and is taken into consideration only together with δ . If $\Omega > 1.1$ and $\delta < 3.6\%$, only solid solutions are formed. If $1.1 < \Omega < 10$ and $3.6\% < \delta < 6.6\%$, only solid solutions and intermetallic compounds are formed, and if $\Omega > 10$, only solid solutions are formed. The calculation formula for Ω Eq. (4) is:

$$\Omega = T_{top} \Delta S_{am} / |\Delta H_{am}| \quad (4)$$

where T_{top} is the melting temperature calculated using the expression Eq. (5):

$$T_{top} = \sum c_i T_{top i} \quad (5)$$

where $T_{top i}$ is the melting temperature of element i.

- The difference in electronegativity $\Delta\chi$ (according to Allen) of the various components of the alloy must be comprised between 3 and 6% in order to form only solid solutions. The calculation formula was deduced in a similar way to the one used to calculate the difference in atomic radius Eq. (6):

$$\Delta\chi = 100 \sqrt{\sum c_i \left(1 - \frac{\chi_i}{\bar{\chi}}\right)^2} \quad (6)$$

where χ_i is the electronegativity of the element i , and $\bar{\chi}$ is the average electronegativity.

- The critical correlation ratio to obtain only solid solutions is determined by the expression Eq. (7):

$$k_1^{cr} = 1 - \frac{T_A \Delta S_{am}}{\Delta H_{am}} (1 - k_2) > \frac{\Delta H_{IM}}{\Delta H_{am}} \quad (7)$$

where IM index refers to intermetallic compounds, while T_A is the homogenization temperature; k_2 index is considered to be 0.6 and represents the ratio between the entropy of the formation of the compounds and that of the formation of solid solutions.

Even though some inconsistencies can be noticed between the above-mentioned criteria, they are useful to evaluate the conditions under which solid phases are formed in multi-component alloys [13, 14].

1.2 State of the art

High entropy alloys with different compositional characteristics have attracted a lot of attention due to their potentially interesting properties for special fields. Meanwhile, this area provides vast opportunities for new compositions and microstructures, especially for complex alloys [15, 16].

After developing refractory high entropy alloys composed of a single BCC phase in W-Nb-Mo-Ta and W-Nb-Mo-Ta-V alloy systems, it was necessary to produce alloys that comprised transitional metals such as Nb-Mo-Ta-W, V-Nb-Mo-Ta-W, Ta-Nb-Hf-Zr-Ti, Hf-Nb-Ta-Ti-Zr, Mo-Nb-Ta-V-W and the equiatomic Hf-Mo-Nb-Ta-Ti-Zr alloys [3, 15–18]. From a biocompatibility perspective, it is interesting to note that the majority of these elements are biocompatible, with the exception of vanadium. By combining the HEA concept with the need to ensure alloy biocompatibility, biocompatible high entropy alloys have been designed from the above-mentioned systems, with potential use for orthopedic implants. Results are reported as regards the production and testing of high entropy alloys in the system TiNbTaZrMo, TiNbTaZrFe, TiNbTaZrW, TiNbTaZrCr, and TiNbTaZrHf having deformability and biocompatibility characteristics superior to pure titanium, considered to be the least cytotoxic of all metals.

The high entropy alloys in the CrCoFeMoMnNiNb system microalloyed with Ta, Ti or Zr have special mechanical characteristics (compression strength above 2000 MPa, good deformation capacity under severe conditions and good dynamic impact behavior), excellent passive film chemical stability (corrosion potential in simulated biological environment), and reduced cytotoxicity (determined within the MTT test, ISO 10993) compared with the classical alloys used in highly demanding medical devices (CoCr or CoCrMo alloys), which have recorded side effects (tissue necrosis and release of metal ions in the body exceeding the acceptable limits) [15].

The data for the VEC parameter (valence atom concentration) from the TiNbTaZr and TiNbTaZrX alloys (where X was the element replaced, in turn, with Cr, V, Mo, W, and Fe) were located around value 5, indicating the formation of a BCC structure as well as the tendency to form a solid solution phase. In accordance with the above-mentioned criteria, the TiNbTaZr and TiNbTaZrX1 alloys (where X1 can be one of the Mo or W elements) show a reduced possibility of solid solution formation due to the high value of the δ parameter (difference of the atomic radius) [18].

Refractory element Mo is preferred in manufacturing metallic biomaterials due to the fact that it can be found in several conventional metallic biomaterials, such as Ti-15Mo-5Zr-3Al and Co-Cr-Mo [15–19]. Cast and quenched HEA TiNbTaZrMo had breaking strength values exceeding 1000 MPa, higher than those of TiNbTaZrHf and Ti6Al4V refractory alloys, but also good deformability. Quenching led to the improvement of TiNbTaZrMo deformability, which was attributed to coarse granulation and/or redistribution of constituent elements in the dendritic and interdendritic regions [15, 18]. The distribution of cells formed on different types of substrates plays a significant role in cellular functions that involve protein migration, proliferation, and synthesis. In osteointegration tests, the osteoblasts formed on cast and quenched HEA TiNbTaZrMo surfaces showed a widespread morphology, fairly similar to the morphology of the cells on the CP-Ti titanium alloy. On the other hand, the osteoblasts formed on the 316 L austenitic stainless steel were smaller and had a less widespread morphology. The results obtained indicated that osteoblasts had a better tendency to develop, contributing significantly to forming the bone matrix in the case of HEA TiNbTaZrMo, with or without heat quenching treatments, the effects being similar to CP-Ti alloys [15, 16].

Further research is necessary in order to clarify the origin of the excellent biocompatibility of HEA TiNbTaZrMo. These results clearly indicate that these alloys are a new class of metallic biomaterials with exceptional characteristics. To conclude, the new TiNbTaZrMo equiatomic biocompatible alloy contains two BCC solid solution-type phases with a fine equiaxial dendritic structure and an excellent biocompatibility compared to pure Ti, together with superior mechanical properties, indicating the possibility of being used as a new class of metallic biomaterials.

Over the last few years, there has been an increased need to manufacture stents to take over blood vessel functions. Alongside the classical titanium alloys used in this respect, some high entropy alloys from the CoCrFeNiMn and Al_{0.1}CoCrFeNi systems were also investigated [16, 20].

CoCrFeNiMn alloy is equiatomic and was developed for the first time by Cantor [17]. He found the alloy to be very stable, to have higher configuration entropy than melting entropy, being made up of a single phase solid solution with FCC crystalline structure [17, 18]. Moreover, it possesses remarkable mechanical properties, such as high plasticity and ductility, as well as significant tear resistance. This alloy's microstructure is dendritic, and its diffusion rates are very slow. This conclusion was reached after carrying out analyses on heat treated specimens at 700 or 900°C for one-hour periods, when it was discovered that the diffusion of elements was extremely low regardless of the value of the holding temperature [20].

The heat treatments led to a moderate increase of the breaking strength from 447 to 515 MPa (in the case of homogenization to 900°C, maintaining the elongation at break at the same value of 51%) for AlCrFeNiMn alloys [17, 18, 20]. The increase of the homogenization time to 48 hours and of the temperature to 1000°C did not produce major changes in the mechanical characteristics, there even being a slight decrease in the breaking strength to 475 MPa and in elongation to 50%. This behavior led to the conclusion that these alloys are not substantially consolidated by precipitating intermetallic compounds during heat treatments. However, different results were obtained by applying a combined treatment that consisted of annealing + rolling + annealing. The heat and mechanical processing parameters were: annealing at 1000°C for 4 hours, cold rolling with a 50% thickness reduction, from 5.8 to 2.9 mm, and a reduction speed of 0.2 mm per passing, followed by a new annealing at 1000°C for 4 hours.

Following the initial annealing treatment, the material loses its hardness, acquires even greater plasticity, and partial diffusion phenomena occur, while the

dendritic microstructure suffers from a rolling finish, reducing interdendritic spaces and eliminating pores and casting defects [17, 20, 21]. The $\text{Al}_{0.1}\text{CoCrFeNi}$ alloy contains 2.44 at % Al and 24.4 at % of elements Co, Cr, Fe, and Ni, respectively, being single-phased with FCC structure. While casting, the mechanical characteristics of this alloy are modest; the yield strength is 140 MPa, the tensile strength is 370 MPa, and the elongation reaches 65%. By applying combined thermo-mechanical treatments (cold rolling with 60% reduction and homogenization at 1000°C for 24 hours) increases in mechanical properties and microstructure modification from dendritic to polygonal are obtained [17, 18].

Combining a Ti oxide layer with a Zr oxide layer in a TiNbTaZr alloy demonstrated an excellent biocompatibility. From this viewpoint, obtaining a high corrosion resistance of the implanted metals, which work under physiological corrosion conditions over long periods of time, became a major concern. The excellent corrosion resistance of HEA TiZrNbTaMo in corrosive environments, comparable to that of the Ti6Al4V, was due to the passivation effects of the surface and to achieve high stability to the pitting phenomenon [21–26]. In general, the biomaterial-made implantable elements are aimed at improving and extending the patients' lives. After using orthopedic prostheses made from bio inert materials for a long time, the emphasis is now laid on using materials that can activate tissue repair mechanisms, called bioactive materials, through phenomena aimed at increasing proliferation and differentiation of osteoblasts, resulting in in situ reformation of bone architecture [27, 28]. Regarding the biocompatibility of implantable alloys, it is mandatory to ensure an increased corrosion resistance in the corrosive physiological environment compared to the classical alloys [18].

This chapter presents a series of results regarding the obtaining and characterization of high entropy biocompatible alloys from the CrFeMoNbTaTiZr, CrFeMoNbTaTi, CrFeMoNbTaZr, CrFeMoTaTiZr, CrFeTaNbTiZr, CrTaNbTiZrMo, and FeTaNbTiZrMo alloying systems. All the alloys were produced at laboratory scale, in an electric-arc remelting furnace in an inert argon atmosphere. Given that the alloys contain easily fusible elements, some of the metal components were not completely melted during the primary processing. The microstructural characteristics and the microhardness of the alloys suffered changes following the application of homogenization heat treatments. Some of these experimental alloys underwent corrosion resistance tests in simulated biological environments, the results obtained being encouraging. The microscopic investigation of cell viability in direct contact with FeMoTaTiZr alloy in a 1:1:1:1 ratio, in which the in vitro cultivation of mesenchymal stem cells isolated from human bone tissue was carried out, demonstrated the biocompatibility of this type of alloy [28]. The conditions of adhesion to the implanted metallic material can be improved by depositing hydroxyapatite-based layers on its surfaces using the magnetron sputtering method. This method allows controlling the deposition parameters so as to obtain thin, flawless, uniform layers, with a very good adhesion to the substrate, low roughness, resistant to corrosion and wear, low stress layers, which are essential properties to be used in medical applications [29].

2. Experimental results

2.1 Obtaining of biocompatible high entropy alloys in the RAV MRF ABJ 900 furnace

High entropy alloys can be obtained in optimum conditions in RAV furnaces working in high purity argon-controlled environments. The concept for the design

of experimental alloy recipes from the CrFeMoNbTaTiZr system was based on the choice of chemical elements having extremely low biotoxicity, currently used as an alloying base for classical alloys used to manufacture medical devices. In order to produce high entropy alloys in the CrFeMoNbTaTiZr system in the MRF ABJ 900 vacuum arc remelting equipment within the ERAMET—SIM, UPB Laboratory, seven classes of different alloys were chosen in which the chemical composition varied, maintaining the equiatomic proportion in each of them, as follows: HEAB 1—CrFeMoNbTaTiZr; HEAB 2—CrFeMoNbTaTi; HEAB 3—CrFeMoNbTaZr; HEAB 4—CrFeMoTaTiZr; HEAB 5—CrFeTaNbTiZr; HEAB 6—CrTaNbTiZrMo; HEAB 7—FeTaNbTiZrMo. Raw materials consisting of elements with purity greater than 99.5 wt % were mechanically processed to be introduced into the RAV equipment, then weighed, and dosed in equiatomic reports (**Table 1**).

For each experimental alloy sample, a metal load constant of approx. 30 g was maintained. The raw materials were deposited on the copper plate of the RAV equipment in an order meant to ensure the quickest possible formation of a metal bath under the action of the electric arc (**Figure 1**). This mode of operation is very important when working with refractory chemical elements. After coupling to the cooling system, the process continued with successive suction until a pressure of 5×10^{-3} mbar was obtained in the working area.

Argon atmosphere (5.3 purity levels) was then introduced, and approx. 8–10 homogenization melts were performed, by rotating the samples, in order to ensure a uniform distribution of the chemical elements in the alloys produced. The high

Alloy	Element, g							Production efficiency, g
	Cr	Fe	Mo	Nb	Ta	Ti	Zr	
HEAB 1 CrFeMoNbTaTiZr	2.55	2.73	4.68	4.54	8.77	2.37	4.38	29.85
HEAB 2 CrFeMoNbTaTi	2.97	3.19	5.47	5.30	10.32	2.74	—	29.91
HEAB 3 CrFeMoNbTaZr	2.74	2.95	5.06	4.90	9.54	—	4.80	29.42
HEAB 4 CrFeMoTaTiZr	2.98	3.20	5.50	—	10.36	2.75	5.21	29.69
HEAB 5 CrFeTaNbTiZr	3.00	3.22	—	5.36	10.42	2.76	5.24	29.72
HEAB 6 CrTaNbTiZrMo	2.78	—	5.13	4.98	9.68	2.56	4.87	29.94
HEAB 7 FeTaNbTiZrMo	—	2.97	5.10	4.94	9.61	2.55	4.83	29.95

Table 1. Mass and production efficiency of biocompatible high entropy alloy batches.

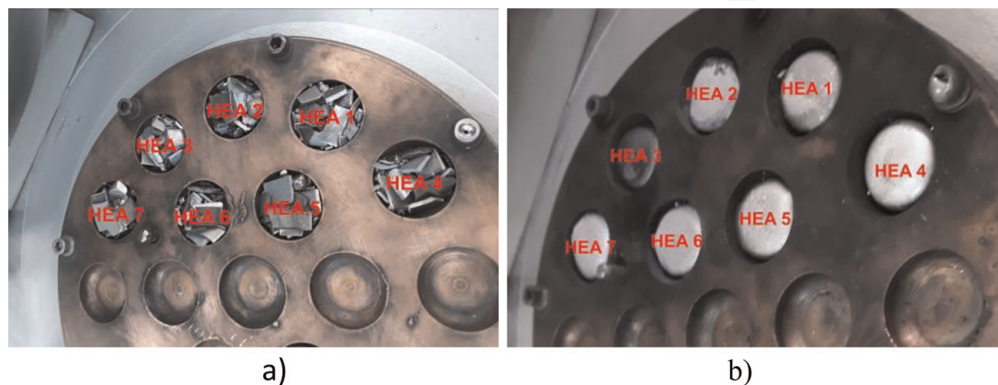


Figure 1. HEAB 1 to HEAB 7 batches prepared for melting on the copper plate of the RAV equipment (a) and after melting (b).

number of successive remelting was imposed by the fact that the load contained high melting temperature elements, such as: Fe—1538°C; Ti—1668°C; Zr—1855°C; Cr—1907°C; Nb—2477°C; Mo—2623°C; Ta—3017°C.

The buttons made from biocompatible HEA alloys (**Figure 1b**) were weighed in order to determine the production coefficient. The losses were due to the fact that, during the process of producing the alloys, there were small drips in the working area, under the action of the electric arc, without their excessive vaporization.

2.2 Microstructure

Samples were taken from the biocompatible high entropy alloys produced in order to carry out the microstructural analysis. The samples taken by abrasive disk cutting under cooling liquid jet were then subjected to the metallographic preparation procedure, using abrasive paper with grit sizes ranging between 360 and 2500, followed by polishing using alpha alumina suspension with grit sizes ranging between 3 and 0.1 μm . The experimental alloys were not chemically etched using metallographic reagents so as to also perform localized chemical composition analyses using the EDAX detector. The microstructural analysis was carried out by optical and scanning electron microscopy, using an Olympus GX 51 optical microscope and a SEM Inspect S electron microscope equipped with an EDAX type Z2e detector from the LAMET, UPB laboratory.

Following the metallographic examination, a significant part of the chemical elements included in the matrix of the HEAB 1 (CrFeMoNbTaTiZr alloy) and HEAB 2 (CrFeMoNbTaTi alloy) was dissolved, forming a solid homogeneous solution (**Figure 2a, b**).

Elements such as Cr, Zr, Fe, and Nb formed a common solid solution in which intermetallic compounds precipitated. Nonetheless, a series of compounds of hard-to-melt elements (Mo and Nb), dispersed relatively uniformly in the base matrix (**Figure 3**), were visible. High melting temperature chemical elements, such as Ta and Mo, were not completely melted, the rounded grains being partially adherent to the solid solution existing between the other chemical elements of the alloy (**Figure 3a, b**). In the case of the HEAB 3 (CrFeMoNbTaZr alloy), the tantalum was impossible to melt within the volume of the designed batch, which was too small. The big difference between the melting temperatures of the chemical elements constituting the alloy, corroborated with the rapid cooling in the water cooled copper base plate, also generated fracture effects in the metal matrix at the interface with the Ta or Mo grains (**Figure 3a, b**).

Even though the HEAB 4 (CrFeMoTaTiZr alloy) contained only two hard-to-melt elements (Mo and Ta), it was still impossible to completely dissolve its metallic grains (**Figure 4a**). Furthermore, between the hard-to-melt metal grain (Ta) and the embedded metal matrix, some micro-cracks were formed perpendicular to the interface, as a result of solidification stresses (in other words, as a result of the inability of the high-hardness metal matrix to disperse the stresses generated by rapid cooling).

The HEAB 5 (CrFeTa NbTiZr alloy) and HEAB 6 (CrTa NbTiZrMo alloy) ran a similar course with the other alloys presented above, the dissolution of the Ta particles being impossible in this case as well (**Figure 4**). A possible cause could be the volume of the grains (having a mass of approx. 10.42 g), which was too big in relation to the total volume of the batch (having a total mass of approx. 29.22 g), which was too small. The very short time in which the alloy was in liquid state did not allow for the complete dissolution of larger grains.

In the case of the HEAB 7 (FeTa NbTiZrMo alloy), the issue of dissolving hard-to-melt metal particles (Ta and Nb) could not be solved during the melting stage

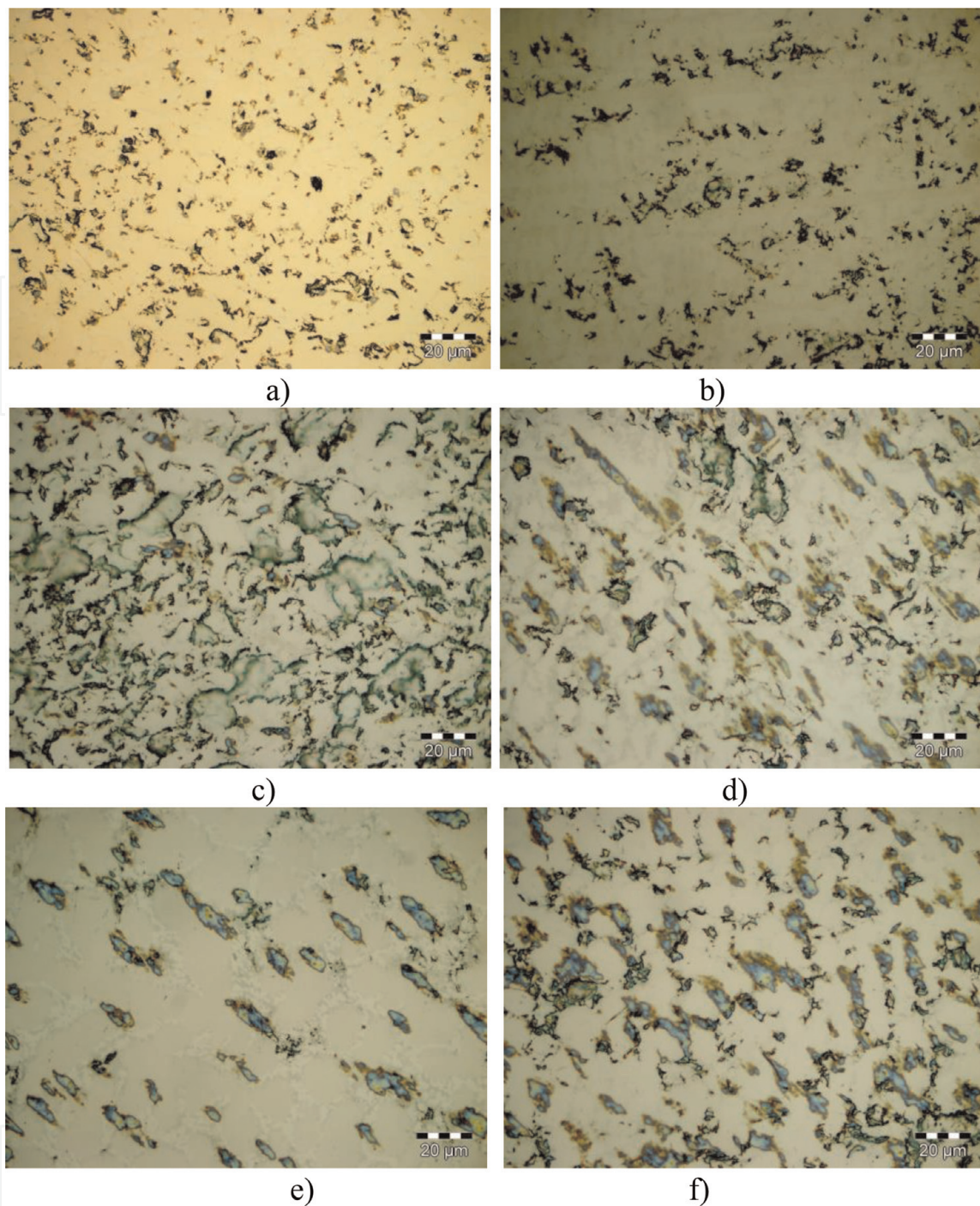


Figure 2. Cross-section of biocompatible HEABs upon the same magnification. Optical microscopy (1000 magnification) (a) CrFeMoNbTaTiZr; (b) CrFeMoNbTaTi; (c) CrFeMoNbTaZr; (d) CrFeMoTaTiZr; (e) CrFeTaNbTiZr; (f) CrTaNbTiZrMo.

(**Figure 5**). The FeTaNbTiZrMo alloy shares characteristics similar to the ones previously mentioned. The Ta particle failed to dissolve in this case as well, a fracture being developed from its interface with the base matrix (**Figure 6**).

The remaining elements formed a fairly homogenous solid solution, with a dendritic appearance, in which a series of intermetallic compounds were dispersed and uniformly distributed. The dendritic appearance of the metallic matrix was also highlighted on the breaking surfaces of the mini ingots (**Figure 7a**). The images obtained with the help of SEM electron microscopy show micro-dendrites alternating with surfaces of cleavage fractures and micro-fractures, which explain the high brittleness of these alloys in cast state. The localized chemical composition analyses

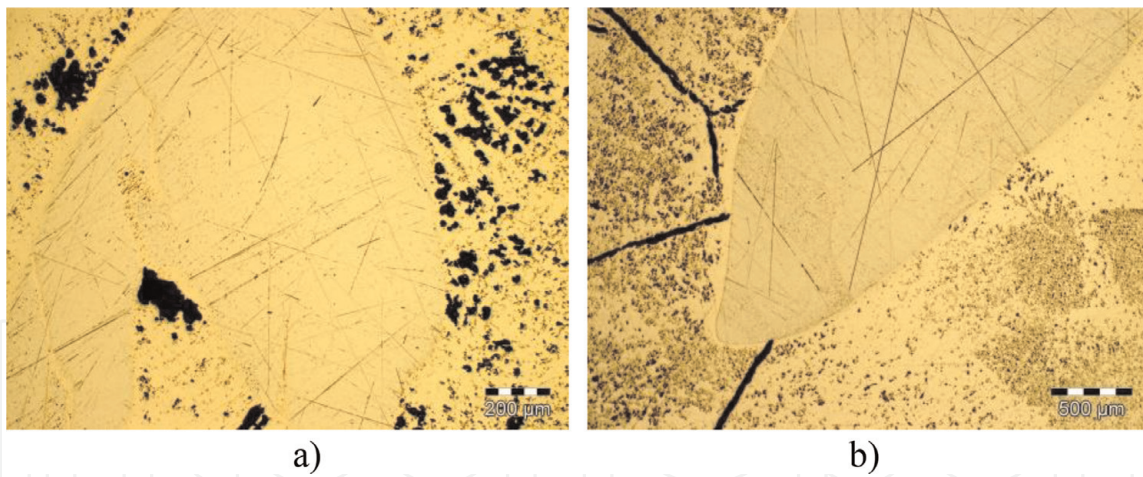


Figure 3.
Undissolved blocks present in the experimental HEAB alloys. (a) CrFeMoNbTaTiZr; (b) CrFeMoNbTaZr.

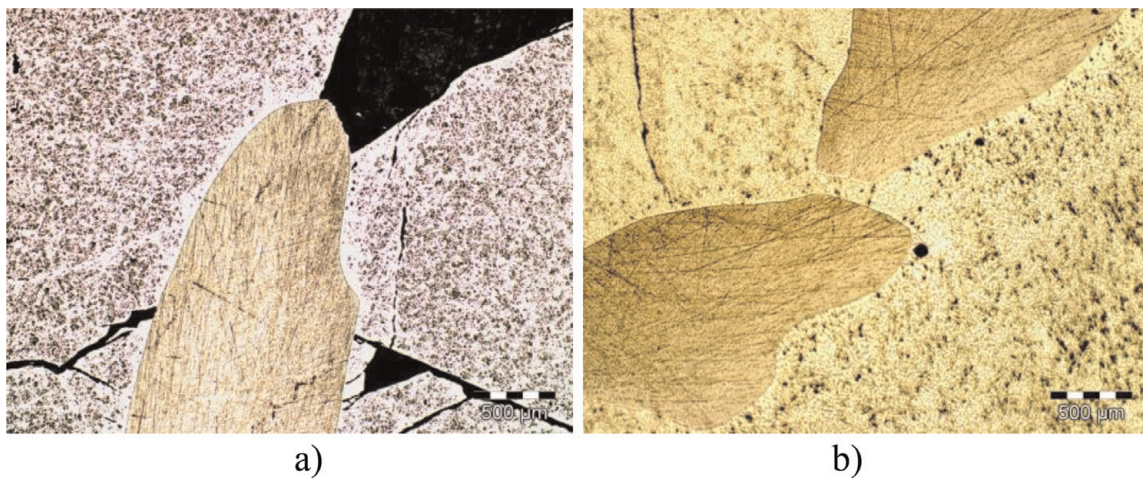


Figure 4.
Undissolved tantalum fragments in the high entropy alloys. (a) CrFeTaNbTiZr; (b) CrTaNbTiZrMo.

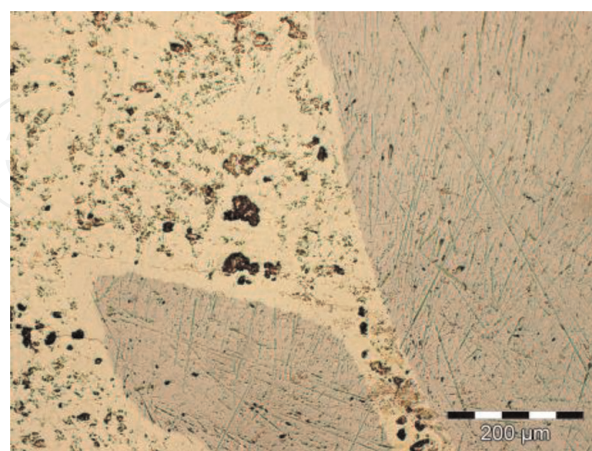


Figure 5.
Undissolved Ta and Nb fragments in the FeTaNbTiZrMo alloy.

(Table 2) highlighted the distribution of elements into the dendritically metallic matrix and the segregation of some elements (Nb, Ti, and Ta) near the interface with undissolved blocks of Nb and Ta (Figure 8).

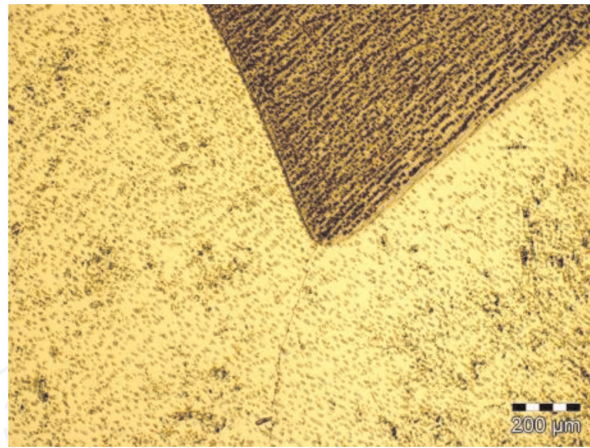


Figure 6.
Undissolved tantalum fragment in the FeTaNbTiZrMo alloy.

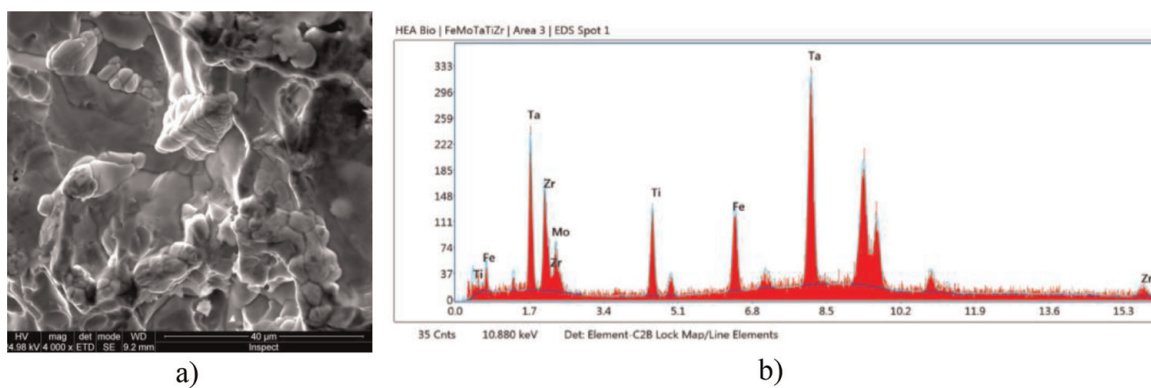


Figure 7.
Microstructure (a) and semi-quantitative composition spectrum (b) of FeTaNbTiZrMo alloy on the breaking surface.

Spot	Chemical elements, wt%						Location
	Fe	Ta	Nb	Ti	Zr	Mo	
1	—	—	100	—	—	—	Nb block
2	—	24.74	67.99	7.28	—	—	Interface with Nb
3	24.19	10.26	14.30	14.25	28.81	8.20	Matrix
4	3.66	25.7	30.00	7.98	5.49	26.90	Matrix
5	—	42.14	48.27	9.59	—	—	Interface with Ta
6	—	100	—	—	—	—	Ta block

Table 2.
The chemical composition of micro-zones which corresponds to **Figure 8**.

2.3 Heat treatments

Given the fact that HEAs are metallic materials with a high degree of chemical heterogeneity resulted from the association of chemical elements with significant differences in atomic diameters and different mutual solubility, the majority of the researchers in the field resorted to applying heat treatments after producing the alloys [20, 21]. The homogenization heat annealing treatments can reduce or eliminate the segregation effects of chemical elements which take place during casting in the case of high entropy alloys [20]. Microstructures near-equilibrium thus results, either by dissolving the metastable phases or by nucleating the equilibrium phases,

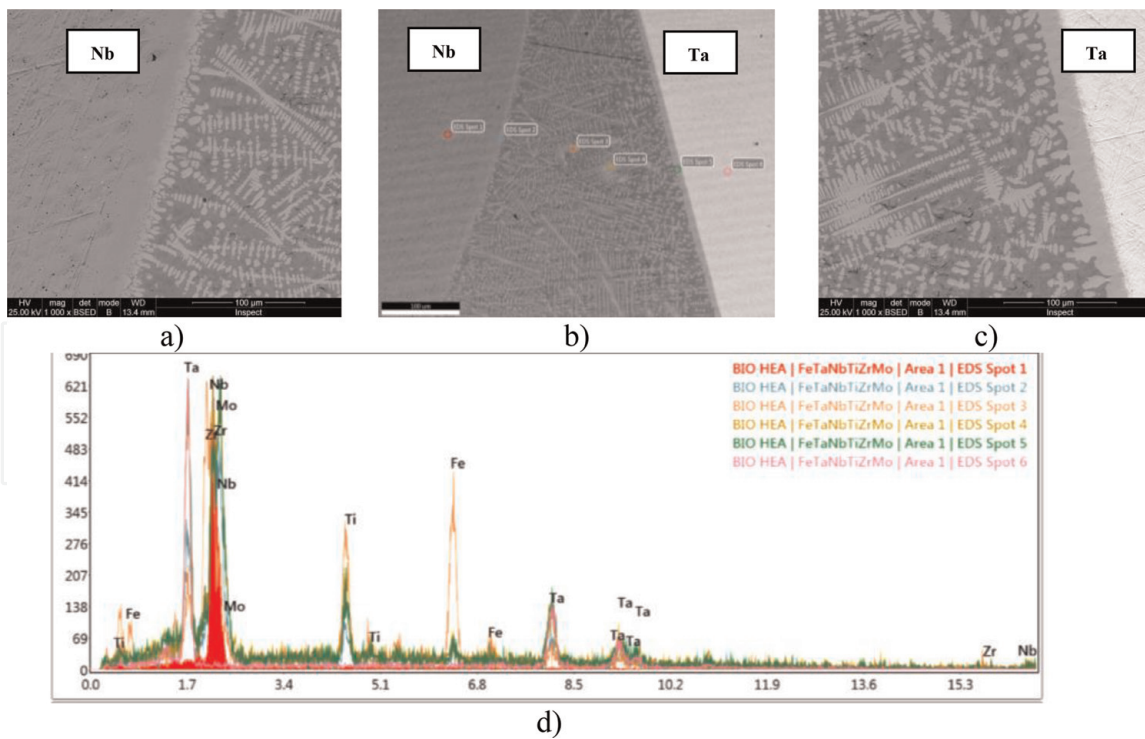


Figure 8. SEM image of interface between two undissolved blocks and dendritically metallic matrix (Nb, a), (Nb and Ta, b), (Ta, c) and semi-quantitative composition spectrum for the FeTaNbTiZrMo alloy (d) for the micro-zones (spot 1 to spot 6).

the formation of which is suppressed during rapid cooling. The final result of annealing treatments is to reduce the level of micro- or macroscopic residual stresses [3, 4]. Thus, homogenization annealing combined with rapid cooling was shown to allow for increased values of mechanical characteristics. In some cases, depending on the chemical composition of the alloy, hardness values decreased if successive heat treatments were applied at different temperatures [1, 22]. Some of the heat treatments applied to high entropy alloys can either lead to hardening effects or to an increased plasticity and toughness, depending on the value of the heating temperature, on the actual duration of holding at those temperatures as well as on the cooling mode. The effects of heat treatments on macro- and micro-structure depending on temperature are very interesting and suggestive [22–30]. The dendritic morphology specific to cast alloys is unaffected if the holding temperature does not exceed 1040°C. On the contrary, when the temperature exceeds 1200°C, phases rich in certain chemical elements occur (e.g., Cu) [20]. The formation of HC-rich in BC-Ta-Nb and hexagonal-packed close (HCP) was highlighted during the heat treatments, depending on the annealing time at 700°C [31].

When it comes to the experimental alloys developed in this chapter, a series of heat treatments were applied in order to achieve the microstructural homogenization and the dissolution of hard-to-melt particles. The samples underwent heat treatment for aging at 600°C for 4 hours and then at 900°C for 6 hours. The heat treatments were performed in the Nabertherm LT 15/12/P320 furnace with a programmable chart for the heat regime. The heating speed was of 20°C/min, and the samples kept for 4 hours were cooled in air, while the samples kept for 6 hours were cooled in the furnace. The evolution of the new alloy microstructure was highlighted by optical and electron microscopy. Thus, before applying heat treatments, the hard-to-melt elements (Ta, Nb, and Mo) did not completely dissolve in the metal melt; they were only diffused at the level of the separation boundaries, on short distances. After the heat treatment, an increased tendency toward oxidation was noticed in the elements located in the superficial layer of the samples, as well as

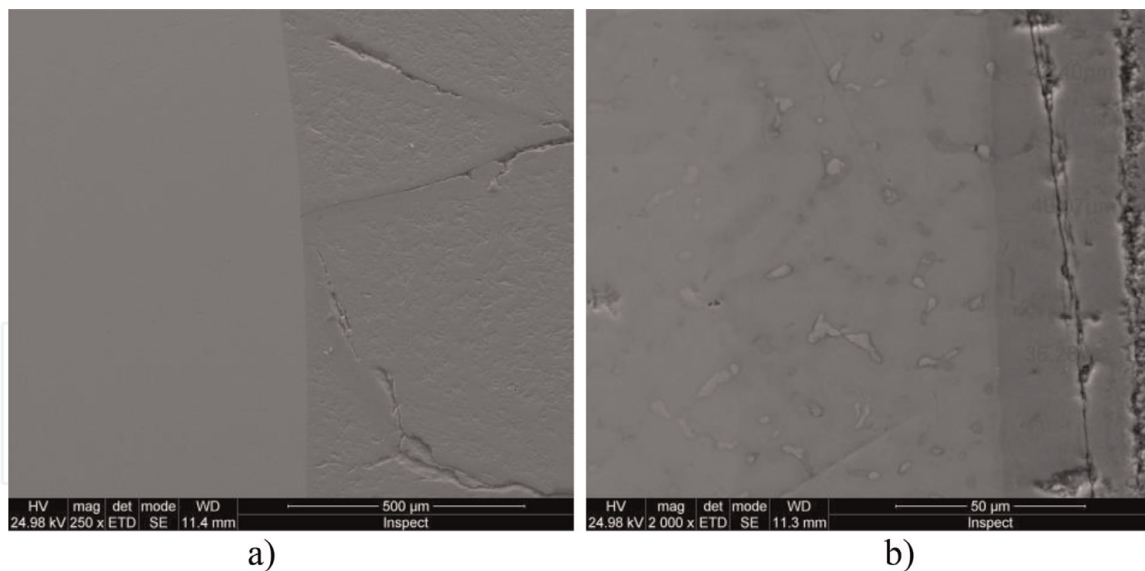


Figure 9.
The oxidized layer of CrFeMoTaTiZr alloy after heat treatment at 800°C/24 hours/slow cooling in the furnace with fractures (a) and peeling (b).

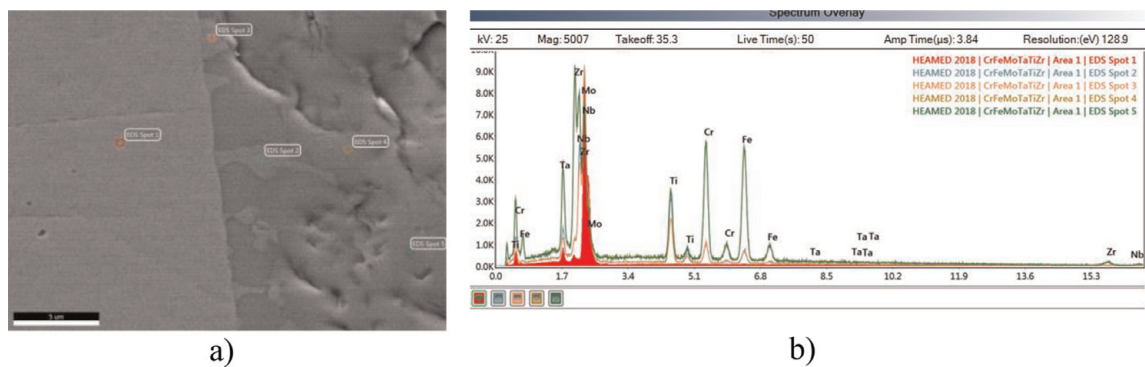


Figure 10.
The interface with undissolved Ta particle (a) and semi-quantitative composition spectrum (b) of the heat-treated CrFeMoTaTiZr alloy.

the formation of a homogenized alloy band, with a dendritic microstructure, located immediately below the complex oxide layer (**Figure 9**).

The effects of the heat treatment are also highlighted by means of an EDS analysis performed with an AMETEC Z2e analyzer on micro-zones located both at the center of the CrFeMoTaTiZr samples as well as at the edges, in order to quantify the oxidation and diffusion effects. An image of the boundary between an undissolved Ta particle and the embedding metal matrix is illustrated in **Figure 10**.

3. Microhardness

The heat treatment effects on mechanical hardness characteristics are highlighted by the different microhardness values determined with the help of the Shimadzu HMV 2 T microhardness tester, presented in **Table 3**.

The analysis of the microhardness values resulted from applying a homogenization treatment showed that hardness increases in the highly alloyed metal matrix up to the average value of 1290 HV0.2 in case of the CrFeMoTaTiZr alloy. The diffusion of the chemical elements during the treatment determined a reduced hardness in the marginal zone adjacent to the surface (located at a distance of approx. 200

Alloy	Microhardness values in points of HV0.2/10	Average value, HV 0.2	Variation coefficient of hardness
CrFeMoNbTaTiZr	749; 739; 700; 743; 747	736	2.76
CrFeMoNbTaTi	750; 732; 747; 804; 736	754	3.85
CrFeMoNbTaZr	775; 748; 719; 725; 803	754	4.66
CrFeMoTaTiZr	697; 764; 795; 790; 712	752	5.97
CrFeMTaNbTiZr	749; 700; 748; 736; 705	728	3.24
CrTaNbTiZrMo	581; 567; 591; 590; 544	575	3.42
FeTaNbTiZrMo	626; 686; 655; 657; 651	655	3.26
CrFeMoNbTiZr	791; 832; 817; 775; 772	797	3.30
Central zone	801; 809; 822; 798; 815	809	1.22
Marginal zone			
Heat-treated	974; 1349; 1406; 1286; 1434	1290	14.38
CrFeMoTaTiZr	906; 876; 893; 893; 840	882	2.88
Central zone	1296; 1429; 1305; 1339; 1316	1337	4.03
Marginal zone			
homogenized layer			

Table 3.
 Microhardness values for biomedical HEA samples.

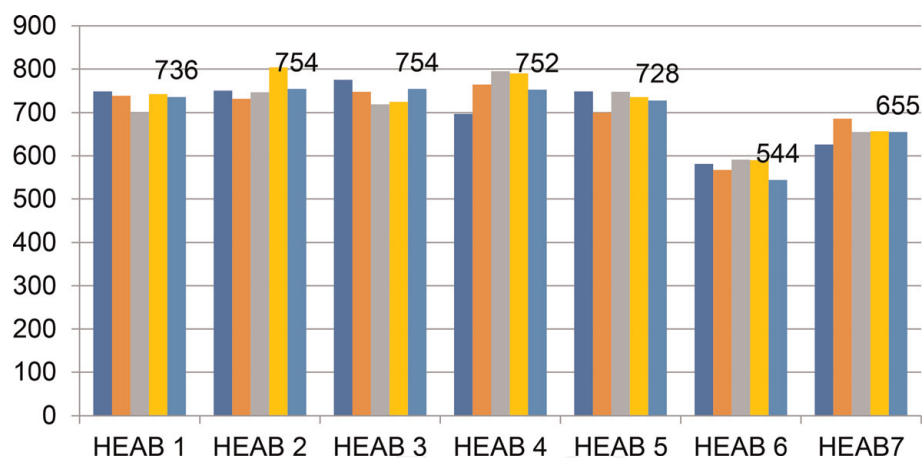


Figure 11.
 Evolution of microhardness for experimental biocompatible HEA.

microns), where the average hardness value was 882 HV0.2, that is, approx. 66 HRC, as well as the formation of a homogenization band of approx. 45 microns, where the hardness increased to 1337 HV0.2. The microstructural aspects are in accordance with the microhardness values.

As can be seen from the data presented in **Table 3** and **Figure 11**, HEAB 1–HEAB 5 have very close values of microhardness, with the average being around 750 HV0.2. A notable difference was obtained with the HEAB 6 alloy, which had the lowest hardness value (544 HV0.2) before heat treatment. Also, for the HEAB 7 alloy, the microhardness was between the minimum and maximum values of the other materials (655 HV 0.2).

After heat treatment, the HEAB 6 alloy recorded a considerable increase in hardness in some areas (under the oxidized layer), which came to about 1337 HV0.2. This development, which represents an increase of over 150%, can be exploited in terms of obtaining high-wear-resistant surfaces for medical instruments.

4. Cell viability preliminary tests

In order to evaluate the cell viability of the new alloys with high entropy in simulated biological environments, a series of experiments on bone fragments taken from bone extractions from human patients were performed. Bone fragments were transferred to minimally modified Dulbecco essential medium (DMEM) (Sigma cat. No. D6046) supplemented to the final concentration of 1% with penicillin/streptomycin (Sigma cat.no.P4333) and 10% fetal bovine serum (FBS) (Sigma F7524) and centrifuged at 4000 rpm for 10 min to dislodge stem cells. Bone fragments were cultured as explants in a vial with a surface of 75 cm² (Eppendorf No. 0030711122) at 37°C, in a humid atmosphere, with 5% CO₂. After 7–10 days, the first cells that migrated from the explants were observed under the microscope. Cells directly in contact with the alloy samples were analyzed in the Leica DMI8 inverted microscope, using FITC and Rhodamine fluorescence cubes, after incubation with Calcein AM and Propidium Iodide.

5. Conclusion

The high entropy alloys in the CrFeMoNbTaTiZr, CrFeMoNbTaTi, CrFeMoNbTaZr, CrFeMoTaTiZr, CrFeTaNbTiZr, CrTaNbTiZrMo, and FeTaNbTiZrMo alloying systems can be produced in the RAV furnace provided that the batch volume is large enough to allow the dissolution of hard-to-melt elements. Raw materials need to be introduced in the form of smaller grain particles (below 1 mm in diameter) in order to favor the dissolution phenomena by diffusion in the common molten metal bath. Moreover, the liquid state holding time must be increased so as to achieve the complete dissolution of particles from hard-to-melt elements. Heat treatments produce superficial oxidation effects, forming oxide layers of approx. 42 microns thick, partly fractured or peeled. The hardness value in case of the CrFeMoTaTiZr alloy increased from 800 HV0.2 to approx. 1290 HV0.2 after applying the heat treatment. The epifluorescence microscopy technique showed that mesenchymal stem cells adhered to the surface of the alloy.

Acknowledgements

The researches were financed by the Executive Agency for Higher Education, Research, Development and Innovation (CNCS CCDI—UEFISCDI), under the grant project no. PN-III-P1-1.2-PCCDI-2017-239/60PCCDI 2018—Obtaining and expertise of new biocompatible materials for medical applications—MedicalMetMat within PNCDI III.

Thanks

The authors would like to thank their colleagues and collaborators Mirela Codescu, Alina Vlădescu, Hajnal Kelemen, Sanda Manu, and Dumitru Mitrică for their contribution to the testing and characterization of experimental materials.

IntechOpen

IntechOpen

Author details

Victor Geanta¹, Ionelia Voiculescu^{1*}, Petrica Vizureanu² and Andrei Victor Sandu²

1 University Politehnica of Bucharest, Bucharest, Romania

2 Gheorghe Asachi Technical University of Iasi, Romania

*Address all correspondence to: ioneliav@yahoo.co.uk

IntechOpen

© 2019 The Author(s). Licensee IntechOpen. This chapter is distributed under the terms of the Creative Commons Attribution License (<http://creativecommons.org/licenses/by/3.0>), which permits unrestricted use, distribution, and reproduction in any medium, provided the original work is properly cited. 

References

- [1] Yeh J, Chen SK, Lin S, Gan JY, Chin TS, Shun TT, et al. Nanostructured high entropy alloys with multiple component elements: Novel alloy design concepts and outcomes. *Advanced Engineering Materials*. 2004;**6**:299-303
- [2] Zhang Y et al. Microstructures and properties of high-entropy alloys. *Progress in Materials Science*. 2014;**61**:1-93
- [3] Tsai M-H, Yeh J-W. High-entropy alloys: A critical review. *Materials Research Letters*. 2014;**2**(3):107-123. DOI: 10.1080/21663831.2014.912690
- [4] Miracle DB, Miller JD, Senkov ON, Woodward C, Uchic MD, Tiley J. Exploration and development of high entropy alloys for structural applications. *Entropy*. 2014;**16**:494-525. DOI: 10.3390/e16010494
- [5] Tang Z, Huang L, He W, Liaw PK. Alloying and processing effects on the aqueous corrosion behavior of high-entropy alloys. *Entropy*. 2014;**16**: 895-911. DOI: 10.3390/e16020895
- [6] Geantă V, Voiculescu I, Miloşan I, Istrate B, Mateş IM. Chemical composition influence on microhardness, microstructure and phase morphology of $Al_xCrFeCoNi$ high entropy alloys. *Revista de Chimie*. 2018; **69**(4):798-801
- [7] Geantă V, Voiculescu I, Ştefănoiu R, Chereches T, Zecheru T, Matache L, et al. Dynamic impact behaviour of high entropy alloys used in the military domain Euroinvent ICIR 2018. *IOP Conference Series: Materials Science and Engineering*. 2018;**374**:012041. DOI: 10.1088/1757-899X/374/1/012041
- [8] Geantă V, Voiculescu I, Istrate B, Vrânceanu D, Ciocoiu R, Cotruţ C. The influence of chromium content on the structural and mechanical properties of $AlCr_xFeCoNi$ high entropy alloys. *International Journal of Engineering Research in Africa*. 2018;**37**:23-28
- [9] Voiculescu I, Geanta V, Vasile IM, Ştefănoiu R, Tonoiu M. Characterisation of weld deposits using as filler metal a high entropy alloy. *Journal of Optoelectronics and Advanced Materials*. 2013;**15**(7-8):650-654
- [10] Voiculescu I, Geantă V, Ştefănoiu R, Patroi D, Binchiciu H. Influence of the chemical composition on the microstructure and microhardness of $AlCrFeCoNi$ high entropy alloy. *Revista de Chimie*. 2013;**64**(12):1441-1444
- [11] Geantă V et al. Virtual testing of composite structures made of high entropy alloys and steel. *Metals*. 2017;**7**: 496
- [12] Csaki I et al. Researches regarding the processing technique impact on the chemical composition, microstructure and hardness of $AlCrFeCoNi$ high entropy alloy. *Revista de Chimie*. 2016; **67**(7):1373-1377
- [13] Fazakas E et al. Microstructure, thermal, and corrosion behavior of the $AlAgCuNiSnTi$ Equiatomic multicomponent alloy. *Materials*. 2019; **12**(6):926
- [14] Popescu G., et al. New $TiZrNbTaFe$ high entropy alloy used for medical, *IOP Conference Series: Materials Science and Engineering* 2018;**400**:022049. DOI: 10.1088/1757-899X/400/2/022049
- [15] Todai M, Nagase T, Hori T, Matsugaki A, Sekita A, Nakano T. Novel $TiNbTaZrMo$ high-entropy alloys for metallic biomaterials. *Scripta Materialia*. 2017;**129**:65-68
- [16] Saini M, Singh Y, Arora P, Arora V, Jain K. Implant biomaterials: A comprehensive review. *World Journal of Clinical Cases*. 2015;**3**(1):52-57

- [17] Cantor B, Chang ITH, Knight P, Vincent AJB. Microstructural development in equiatomic multicomponent alloys. *Materials Science and Engineering A*. 2004; **375–377**:213-218
- [18] Wang S-P, Xu J. TiZrNbTaMo high-entropy alloy designed for orthopedic implants: As-cast microstructure and mechanical properties. *Materials Science and Engineering C*. 2017;**73**: 80-89
- [19] Minciună MG, Vizureanu P, Geantă V, Voiculescu I, Sandu AV, Achiței DC, et al. Effect of Si on the mechanical properties of biomedical CoCrMo alloy. *Revista de Chimie*. 2015; **66**(6):891-894
- [20] Voiculescu I, Geanta V, Ionescu M. Effects of heat treatments on the microstructure and microhardness of AlxCrFeNiMn alloys. *Annals of “Dunarea de Jos” University of Galati, Fascicle XII, Welding Equipment and Technology*. 2015;**26**:5-11
- [21] Munitz A, Kaufman MJ, Nahmany M, Derimow N, Abbaschian R. Microstructure and mechanical properties of heat treated Al_{1.25}CoCrCuFeNi high entropy alloys. *Materials Science and Engineering A*. 2018;**714**:146-159
- [22] Kambic HE. Changing strategies for biomaterials and biotechnology. In: Kambic HE, Yokobory AT Jr, editors. *Biomaterials Mechanical Properties, ASTM STP 173*. Philadelphia: American Society for Testing and Materials; 1994. pp. 293-301
- [23] Hildenbrand H. Biomaterials—A history of 7000 years. *BioNanoMaterials*. 2013;**14**(3–4): 119-133. DOI: 10.1515/BNM-2013-0014
- [24] Balaban DP. *Biomaterials*. Constanța, Romania: Ovidius University Press; 2005
- [25] Williams DF. Definition in biomaterials. In: *Progress in Biomedical Engineering*. Amsterdam: Elsevier; 1987. p. 67
- [26] Williams DF. On the nature of biomaterials. *Biomaterials*. 2009;**30**: 5897-5909
- [27] Floroian L, Badea M, țamotă I. Biomaterials with applications in medicine. *JMB*. nr. 1. 2015. Project POSDRU/159/1.5/S/134378
- [28] Geanta V, Voiculescu I, et al. Grant project no. PN-III-P1–1.2-PCCDI-2017-239/60PCCDI 2018. Obtaining and expertise of new biocompatible materials for medical applications. *MedicalMetMat within PNCDI III, Romania*
- [29] Gao L, Liao W, Zhang H, Utama Surjadi J, Sun D, Lu Y. Microstructure, mechanical and corrosion behaviors of CoCrFeNiAl_{0.3} high entropy alloy (HEA) films. *Coatings*. 2017;**7**:156. DOI: 10.3390/coatings7100156
- [30] Munitz A, Salhov S, Guttmann G, Derimow N, Nahmany M. Heat treatment influence on the microstructure and mechanical properties of AlCrFeNiTi_{0.5} high entropy alloys. *Materials Science and Engineering A*. 2019;**742**:1-14
- [31] Chen SY et al. Phase transformations of HfNbTaTiZr high-entropy alloy at intermediate temperatures. *Scripta Materialia*. 2019; **158**:50-56